Computers in Biology and Medicine 168 (2024) 107713

Contents lists available at ScienceDirect

Computers in Biology and Medicine

journal homepage: www.elsevier.com/locate/compbiomed

Novel methodology for detecting and localizing cancer area in histopathological images based on overlapping patches

Sergio Ortiz [a], Ignacio Rojas-Valenzuela [a], Fernando Rojas [a], Olga Valenzuela [b], Luis Javier Herrera [a], Ignacio Rojas [a,*]

[a] Department of Computer Architecture and Technology, University of Granada, E.T.S. de Ingenierías Informática y de Telecomunicación, C/ Periodista Daniel Saucedo Aranda S/N CP:18071 Granada, Spain

[b] Department of Applied Mathematics, University of Granada, Facultad de Ciencias, Avenida de la Fuente Nueva S/N CP:18071 Granada, Spain

ARTICLE INFO

Keywords:
Deep learning
Artificial intelligence
Medical imaging
Convolutional neural networks
Whole slide imaging

ABSTRACT

Cancer disease is one of the most important pathologies in the world, as it causes the death of millions of people, and the cure of this disease is limited in most cases. Rapid spread is one of the most important features of this disease, so many efforts are focused on its early-stage detection and localization. Medicine has made numerous advances in the recent decades with the help of artificial intelligence (AI), reducing costs and saving time. In this paper, deep learning models (DL) are used to present a novel method for detecting and localizing cancerous zones in WSI images, using tissue patch overlay to improve performance results. A novel overlapping methodology is proposed and discussed, together with different alternatives to evaluate the labels of the patches overlapping in the same zone to improve detection performance. The goal is to strengthen the labeling of different areas of an image with multiple overlapping patch testing. The results show that the proposed method improves the traditional framework and provides a different approach to cancer detection. The proposed method, based on applying 3x3 step 2 average pooling filters on overlapping patch labels, provides a better result with a 12.9% correction percentage for misclassified patches on the HUP dataset and 15.8% on the CINIJ dataset. In addition, a filter is implemented to correct isolated patches that were also misclassified. Finally, a CNN decision threshold study is performed to analyze the impact of the threshold value on the accuracy of the model. The alteration of the threshold decision along with the filter for isolated patches and the proposed method for overlapping patches, corrects about 20% of the patches that are mislabeled in the traditional method. As a whole, the proposed method achieves an accuracy rate of 94.6%. The code is available at https://github.com/sergioortiz26/Cancer_overlapping_filter_WSI_images.

1. Introduction

Cancer disease is one of the most tricky pathologies in the world of medicine [1,2]. Cancer is a disease in which the cells of a certain part of the body grow uncontrollably and move to invade another part of the body. The normal cells grow and reproduce through the process of cell division to give new cells to the body [3].

In 2020, 19.3 million cases of cancer have been estimated, of which almost 10 million have ended in death. Breast cancer has become the greatest impact cancer ahead of lung cancer. The five main cancers are breast cancer (11.7%), lung cancer (11.4%), followed by colorectal (10.0%), liver (8.3%), and stomach cancer (7.7%) [4]. Nevertheless, breast cancer is not the cancer with the highest mortality, but lung cancer with approximately 1.8 million deaths (18%) [5]. Breast cancer is one of the most malignant cancers in women, being the most important in terms of the new cases worldwide [4]. As presented in [6], the estimated number of new breast cancer cases in the United States in 2023 is 297 790, being breast cancer the most common cancer diagnosed in women (31% of all cancer cases in women diagnosed in the USA). In spite of this, among females is the leading cause of cancer death (43 170 estimated cases in the United States in 2023 [6]), and the incidence rates greatly exceed the limit concerning his followers [6,7].

Cancer is a disease that can quickly spread to other parts of the body. For this reason, the first step in cancer detection by a pathologist is to examine the cells in the histological section and identify the tumor cells. The problem with delineating the tumor tissue on the images is mainly the time consuming and monotonous nature of the procedure. For this reason histological imaging in conjunction with Deep Learning (DL) is a powerful tool to detect cancer cells and localize them throughout the image [8–10]. Whole Slide Imaging (WSI) offers

* Corresponding author.
E-mail addresses: sergioortiz1@correo.ugr.es (S. Ortiz), irojas@ugr.es (I. Rojas).

https://doi.org/10.1016/j.compbiomed.2023.107713
Received 25 October 2022; Received in revised form 7 November 2023; Accepted 15 November 2023
Available online 19 November 2023

promising insight into tissue information collection, promising now and in the future, [11,12].

Early detection of cancer offers great advantages for patient therapy and treatment [13–15]. However, such early detection requires efficient and rapid techniques to analyze both healthy patients and possible new cases to obtain a timely diagnosis using the least invasive techniques [16]. For this purpose, histopathological examinations are an appropriate method to establish a diagnosis [17–20]. Many research efforts have focused on the detection of cancer in the early phase, just as the detection of the zone where the cancer is located [21–24].

Image analysis (currently using intelligent systems on advanced computer platforms [25,26]) can be used to examine tissue samples previously obtained through a chemical-biological process of extraction and staining of the same, in order to improve contrasts and contribute to appropriate medical diagnosis in some cases and analysis of biological processes in others. With the help of digital microscopes, it is possible to obtain digital images of tissue samples that can then be analyzed on a computer, which was previously done manually by a radiologist. These decision support systems, often based on artificial intelligence (Computer-Aided Diagnosis, CAD) [27–29], do not replace the human expert (in our case the pathologist, oncologist or medical specialist), but they are a powerful aid tool in diagnosis automatic, characterization and knowledge of medical images [30].

Accurate detection of the histopathological image area containing cancer cells is of great help to medical experts in the field of cancer diagnosis. The technology makes it possible to detect and locate cancerous areas and bring them to the attention of specialists using CAD systems.

This paper presents a method for detecting breast cancer disease and localizing the area in a tissue image. The method used is based on detecting cancer in small patches of tissue, and by a process of patch overlay localizing where the regions of disease are located in the whole images (on hematoxylin and eosin-stained whole-slide images).

2. Related work

Due to the important and powerful role of deep learning and machine learning in recent years, computer-aided diagnostic systems are essential in the fight against various health pathologies, including cancer [42–44]. Numerous professionals have therefore put all their efforts into research with these methodologies, to improve the disease, translating these advances into scientific publications. The studies of the different authors are based on the detection of cancer and the localization of the area where it is located.

Angel Cruz-Roa et al. [31] realized research about invasive breast cancer detection in WSI, identifying automatically cancer and achieving a Dice coefficient of 75.86%, a positive predictive value of 71.62%, and a negative predictive value of 96.77% in terms of pixel-by-pixel. Dayong Wang et al. [32] realized a deep learning algorithm to identify metastatic breast cancer and achieved an AUC of 0.925 in WSI classification and a tumor location score of 0.733. Besides this, the result of his investigation combined with the human pathologist's diagnoses increased the pathologist's AUC to 0.995. Sumaiya Dabeer et al. [33] proposed the training of a convolutional neural network to detect malignant or benign images, and achieved a prediction accuracy of 93.45%, precision of 93%, and recall of 93%. Kun fa et al. [34] proposed a deep learning method for the detection of cancer metastases in WSI which achieved an AUC score of 90.23%. Erkan Deniz et al. [35] do use transfer learning to detect breast cancer. The method is based on obtained features of histopathologic images through to AlexNet and Vgg16 models and then classified by support vector machines (SVM). The accuracy result obtained for different magnification factors are 90.96% for 40x, 90.58% for 100x, 91% for 200x and 91.30% for 400x. Shallu Sharma et al. [36] realized a Multi-classification of breast cancer histopathology images using existing networks (VGG16, VGG19, and ResNet50) as feature extractors and SVM as end classifier. The accuracies for patch detection were 93.97% for 40×, 92.92% for 100×, 91.23% for 200×, and 91.79% for 400×. Noorul Wahab et al. [37] proposed a Multifaceted fused-CNN with the finality of selecting the region of interest (ROI) due to the very large sizes of WSIs, getting a result of 0.582 in terms of Cohen's Kappa. Table 1 shows a summary of different methodologies presented in the bibliography.

A popular dataset in the field of public histopathological breast cancer imaging is the data presented in [45], called BreaKHis. It consists of 7909 histopathological images of breast cancer, 2480 benign and 5429 malignant specimens, from 82 patients at different magnification factors. In the study conducted by [38] on the BreaKHis dataset, a new deep learning model based on a convolutional neural network is presented. The classification success was increased by using the model called BreastNet. The general structure of the BreastNet model is a residual architecture built on attention modules.All image data is processed using augmentation techniques before being used as input to the model. With the augmentation techniques, each image is processed individually and transferred to BreastNet. Gour et al. [39] presented a novel 152-layer convolutional neural network based on residual learning, called ResHist, for the classification of histopathological images of breast cancer, using the BreaKHis dataset. The ResHist model learns rich and discriminative features from histopathological images and classifies them into benign and malignant, performing superior to other Deep Learning frameworks presented in the literature (such as AlexNet, GoogleNet, VGG16 or VGG19). The authors, however, point out the need to consolidate the results with more and larger datasets.

The authors of the paper [40] presented a fine-grained classification and grading model. The improved fine-grained pathological image classification model was based on the standard deep learning framework called Xception network. In order to further improve the classification accuracy, the multi-class recognition task and the image pair verification task are combined in the process of representation learning.

Both the BreaKHis, VLAD [46] and LSC [47] datasets were used. The authors of the paper [41] propose a hybrid methodology, that combines different machine learning tools, such as weighted feature selection, bio-inspired genetic algorithms and a Convolutional Neural Network. The feature selection method was used to select a combination of the best textural, graphical and morphological features. The genetic algorithm was responsible for optimizing the whole classification system, resulting in a high computational cost.

Alruwaili and Gouda [48] presented two alternatives for breast cancer diagnosis, in a binary problem, using the MIAS database. MIAS is an organization of scientific groups in the UK concerned with mammogram perception. A database of mammographic images collected through London's Royal Marsden Hospital, which includes 322 digitized films, and 2.3 GB of 8 mm are available [49].

To improve the intensity of the mammogram image and eliminate any noise, the proposed system employs image enhancement techniques. Two alternative DL approaches, Nasnet-Mobile and MOD-RES, were trained on preprocessed mammography images to avoid overfitting and increase the overall capabilities of the proposed DL systems. The proposed method outperforms professional radiologists with an overall accuracy of 89.5%, an accuracy of 89.5% and an F1-Score of 89.5% using MOD-RES + oversampling.

In this paper, we proposed a novel method of overlap patches to improve the performance results. This process of overlapping patches is implemented with different alternatives to make a decision about the output label. More specifically, for the localization of the disease in a region, all overlapping patches are considered using different filtering methods that assign different weights to the labels of each examined patch. In this way, we have different labels for the same place because this zone is shared for some patches that overlap. The differentiation weights assigned to the various patches containing part of a particular zone are relative to the amount of area in common with the zone under study. More details are explained in section 5. In addition, a filter that corrects isolated patches and modification of the CNN decision threshold is studied to improve performance.

Table 1
Comparative summary of different methodologies presented in the bibliography.

Author, year	Objective	Method	Metrics
Angel Cruz-Roa et al. [31]	Invasive breast cancer detection	ConvNet	DC = 75.86% TPV = 71.62% TNV = 96.77%
Dayong Wang et al. [32]	Identifying Metastatic Breast Cancer	GoogLeNet AlexNet VGG16 FaceNet	AUC = 92.5% Tumor location score = 0.733
Sumaiya Dabeer et al. 2021 [33]	Detect malignant or benign images tissue	CNN	Accuracy = 93.45% Precision = 93% Recall = 93%
Kun fa et al. [34]	Detection of cancer metastases	InceptionV3	AUC = 90.23%
Erkan Deniz et al. [35]	Transfer learning for breast cancer detection (study of magnification factor)	AlexNet VGG16 SVM (deep feature extraction and SVM classification)	Accuracy(40x) = 90.96% Accuracy(100x) = 90.58% Accuracy(200x) = 91% Accuracy(400x) = 91.30%
Shallu Sharma et al. [36]	Multi-Classification of Breast Cancer Histopathology Images	VGG16, VGG19, ResNet50 and SVM	Accuracy(40x) = 93.97% Accuracy(100x) = 92.92% Accuracy(200x) = 91.23% Accuracy(400x) = 91.79%
Noorul Wahab et al. [37]	Selecting region of interest (ROI) in WSI images	Multifaceted fused-CNN	Cohen's Kappa = 0.582
Togacar et al. [38]	Improving the classification accuracy on the BreakHis data, using the proposed (fast) model called BreastNet	Deep Learning, BreastNet, Binary classification	Accuracy(40x) = 97.99% Accuracy(100x) = 97.84% Accuracy(200x) = 98.51% Accuracy(400x) = 95.88%
Gour et al. [39]	Classification of BreakHis data, using ResHist	Residual Deep Learning model with 152-layer convolutional neural network	Accuracy(40x) = 90.69% Accuracy(100x) = 91.12% Accuracy(200x) = 95.36% Accuracy(400x) = 90.24%
Li et al. [40]	Classification and grading model for pathological images	Multi-task CNN. BreaKHis, VLAD and LSC dataset	Accuracy(40x) = 95.13% Accuracy(100x) = 95.21% Accuracy(200x) = 94.09% Accuracy(400x) = 91.42%
Reshma et al. [41]	Hybrid methodology, combining different machine learning tools	Relief, Genetic Algorithm and CNN, for BreaKHis	Accuracy = 89.13% F1S = 85.38%
Alruwaili and Gouda [16]	Image enhancement techniques and Deep Learning Models	Two alternative: Nasnet-Mobile and MOD-RES	Accuracy = 89.5% F1S = 90% AUC = 89.5%
Our novel overlapping method	Detect and located malignant or benign cancer tissue	Densenet CNN	Accuracy: HUP dataset = 94.6% CNIJ dataset = 91.8%

3. Material and methods

3.1. Dataset

In this project, two datasets are used from different sources [31].

- The first dataset is from The Hospital of The University of Pennsylvania (HUP). In this dataset, each image has zones with cancer and zones of normal tissue. The number of images is 235 for this source. Patients in the HUP cohort ranged in age from 20 to 79 years and had invasive breast cancer.
- The second dataset used is the invasive breast cancer patients from the Cancer Institute of New Jersey (CINJ). The dataset was composed of two distinct classes, positive and negative tissue respectively. The number of cohorts is 40 for this dataset, and each cohort was labeled manually by specialized pathologists.

An extensive repository of histopathological images frequently used in the literature can be found in the Dryad [50], linked to the following page: https://datadryad.org/stash/dataset/doi:10.5061/dryad.1g2nt41

Each image in the dataset HUP and CINJ has a size of 3002×2384. These images (HUP and CINJ) were digitized using Aperio scanners. Aperio Digital Pathology Slide Scanners are very commonly used in histopathological imaging [51]. There are others in the literature, such as the Case Western Reserve University (CWRU) images, where the images are digitized with Ventana scanners. In our case, in the two datasets used (HUP and CINJ), the images used are manually annotated by pathologists and the cancerous regions delineated at 2x magnification using again highly professional software, such as Aperio's Image scope v11.2 (see Fig. 1).

3.2. Data augmentation

In this work, several techniques are used for active data enrichment. These techniques aim to make small changes to the images in order to augment the class that has fewer patches. The augmentation techniques are as follows:

- Rotation: allows applying random rotation to images. In this function the range rotation is fixed, being in our case 20 degrees as the maximum rotation.
- Horizontal flip: allows to turn the images over the x-axis.
- Vertical flip: allows to turn the images over the y-axis.
- Zoom range: is used to generate images with several zoom levels.

3.2.1. CNN

In the literature, the main CNNs used to detect cancer are VGG16, ResNet, ConvNet, Inception V3, and Densenet among others. In this

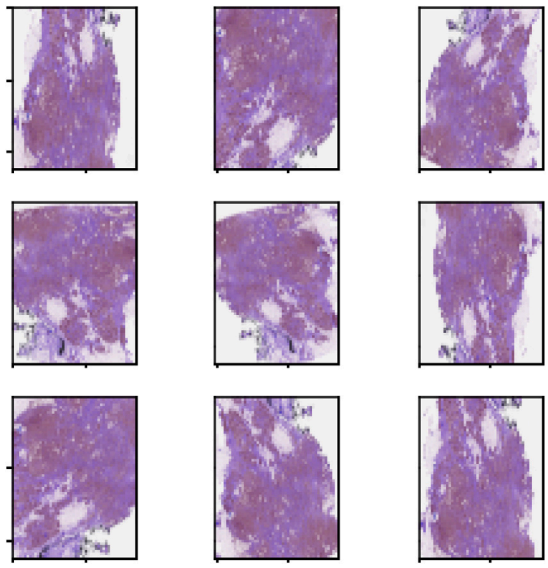

Fig. 1. Data augmentation techniques applied to a patch to visualize the change it produces in the input. The original patch is which appears in Fig. 4.

paper we have performed experiments with Densenet-121, Inception-V3, and VGG16 networks, although the best results were obtained with Densenet CNN, detailing the structure of this one below.

-Densenet

DenseNet (Dense Convolutional Network) is a CNN that uses dense connections between the different layers, via Dense Blocks, that directly connect the layers (with matching feature map sizes) [52]. An important feature is that the layer receives additional inputs from all previous layers and transmits its own feature maps to all subsequent layers. This has the effect of making the model denser and less prone to overfitting [53].

The cross-entropy is the loss function used in the CNNs of this project, whose aim is to minimize the distance between the predicted label and the truth label. The loss function is necessary to estimate the loss of the model to set the weights and to update it to improve the estimate [54].

Traditional metrics such as accuracy, precision, recall, specificity, specificity, and F1 score are used. In addition to these metrics, the main evaluation of the proposed methods is done by assessing the number of misclassified patches that will be able to be corrected by using the overlapping process together with the proposed filters in each case.

4. Process description

The process that has been carried out can be summarized in Fig. 2. This work can be divided into two stages mainly:

Stage (1): the first stage is to create a dataset of patches with two classes 'normal' and 'tumor' (breast cancer). In addition, a CNN is trained to detect cancer in these patches. In the training phase different CNN parameters, are alternated to investigate their influence on the results and to select those that provide the best predictive results.

Stage (2): the second stage is based on the location of the cancer zone in the whole image. In this phase, the CNN trained in stage 1 is used as a basis and implements different methods of overlap patches to improve the predictions of the CNN. In this stage different filters are applied on the label patches overlap, to assign the correct label. The process is based on reinforcing the prediction of a patch by using the surrounding overlapping patches.

As stated above, the first step consists of making the patches dataset, a process that can be described in the Fig. 3.

We start from a database with images that are examined by experts in this type of disease, who with their knowledge are able to isolate the tissue affected by cancer. These expert examinations of the images are recorded in mask images, where different colors select the normal and tumor zone. Once we have both the original images and their mask, positioning the mask over the images allows us to locate the areas with or without cancer.

This paper has used patches of 100 × 100 of the whole image, labeling the path concerning the mask. The mask shows where the areas containing cancer are, areas with white color, and the areas where the tissue is normal, with black color. To label a patch we detect in the mask area whether it has white or not, meaning that the patch belongs to the class normal or tumor. Once we have a dataset with different categories of patches, we endeavour to train a CNN to provide us with the ability to detect new patches with breast cancer and label them for new images. In the training phase, there is no overlap between patches, but individual patches are performed in a continuous process. A total of 47 292 patches were obtained from all the images, of which 32 351 were normal tissue and 14 941 were cancer tissue. To avoid this imbalance in the training, the same number of normal and cancer class patches were chosen, collecting a total of 29 882 patches in the dataset.Thus, all cancerous patches were taken and the same number of normal patches were randomly selected from the normal patches.

It is important to highlight that in our research we only consider a tumor patch if the percentage of cancer in this region is higher than 15% of the total area. We do this because if one patch has for example a 3% of this patch could confuse the training of the CNN. In this way, we facilitate the learning process of the network without neglecting these patches with small proportions of cancer because our developed overlapping process is subsequently applied to them. By doing so, we manage to detect that patch as cancer if it is part of a larger adjacent cancerous area, i.e. if this cancerous zone is part of an adjacent cancerous area of the surrounding patches that share at least 1/4 of tissue with the patch in question . In addition, it is necessary to remove the patches belonging to the background, a process that is described in 4.1.

In stage 1 the CNN learns the characteristics of the different categories in order to predict the label for the future patch. The aim of this learning is to locate the place with cancer in the patient images. Once the CNN weights have been defined, the patches of each complete image are tested in stage 2 to locate the cancer zone. To improve the performance of this phase, a novel method for overlapping patches with different alternatives is proposed. This process is explained in 4.2 and 4.3. In addition, a filter is applied to correct isolated patches, and the decision threshold of the CNN is changed to achieve better results in cancer localization (Sections 4.4 and 4.5).

It should be emphasized that the most novel part of the work is in Stage 2 where we improve the performance of labeling and localization of patches by the proposed novel method. However, Stage 1 completes the previous work of patch dataset generation and CNN characterization through the training and validation stages.

4.1. Pre-processing

In deep learning, it is important to reduce both time and computational overhead and to complete the application as quickly as possible. Since WSI images of cancer diseases have a large resolution, it is relevant to focus the analysis on areas that contain tissue and exclude the background which is usually the white zone around this. To achieve this, we use a method that calculates the channel of RGB representation color, checking the individual three channels in this representation.

A threshold is set to check if the average of each RGB channel of the patch is greater than 230, a value selected considering the RGB color palette. The value of 230 is the best result of the multiple experiments because the background of this type of image is grayish and 230 is a grayish tone in the RGB palette.. In this way, if the three-channel individuals are higher than this value, the color breaks away from the main stream that we want to detect (tissue), this detection color being white or close (background color). See this in Fig. 4.

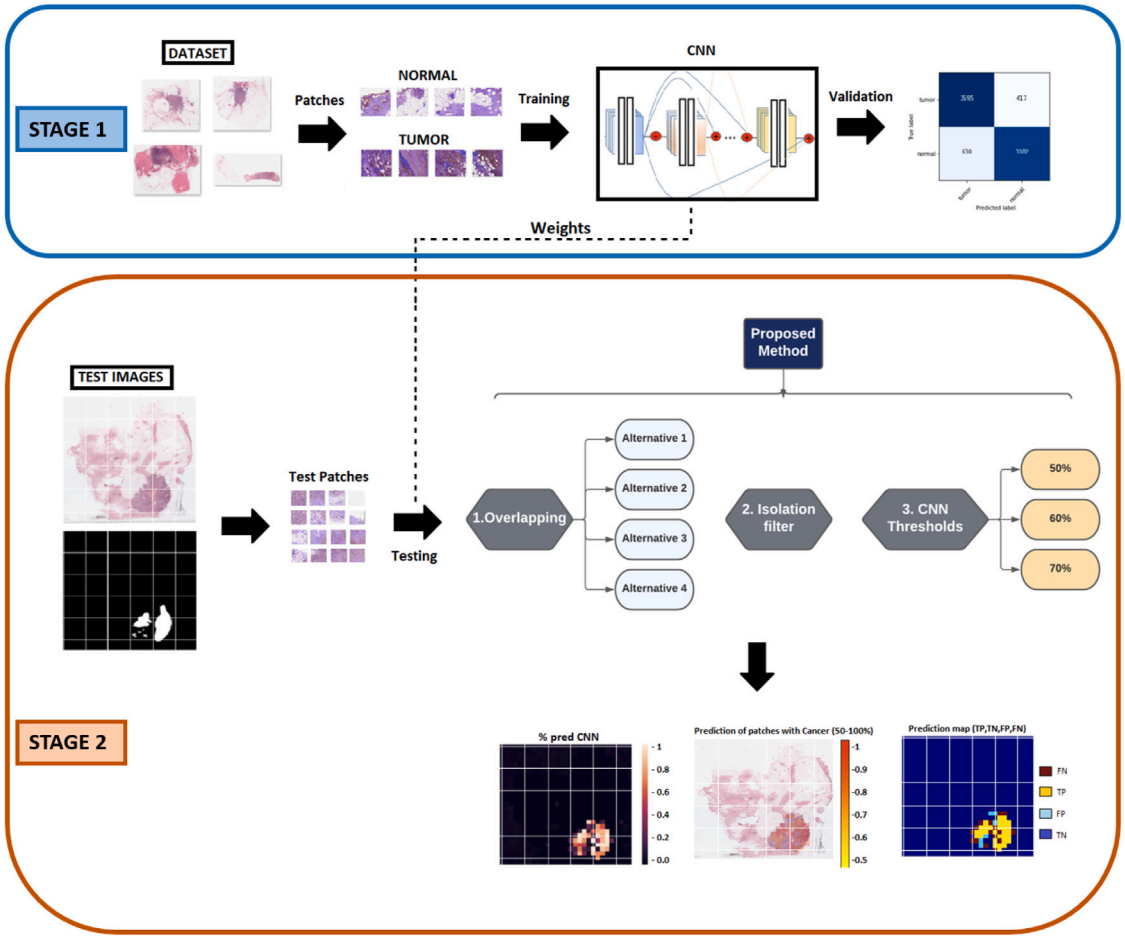

Fig. 2. Diagram detailing the description of the process. The first stage is to create the patch dataset and train and validate the CNN. The second stage is to test new images and predict which patches and areas have cancer disease.

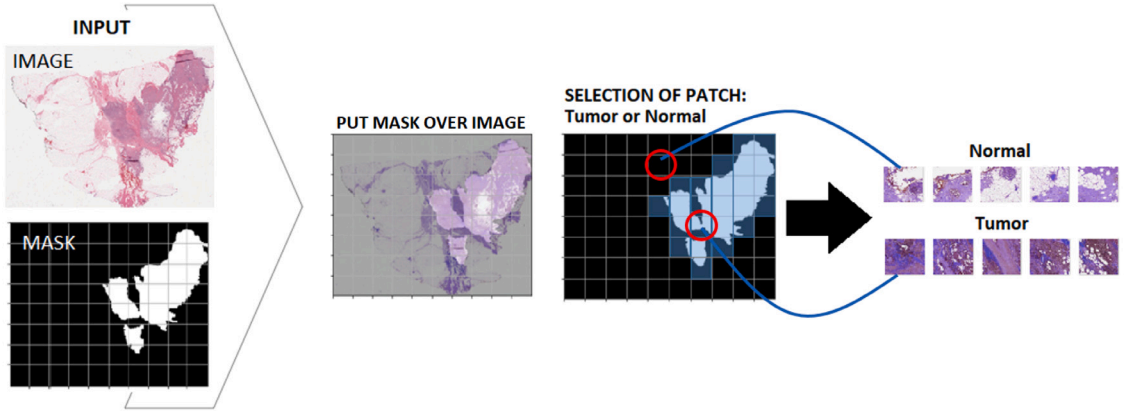

Fig. 3. Process of patches creation and label concerning the mask. The mask remark two different zones in the tissue, the normal tissue (zone black) and the tumor tissue (zone white).

4.2. A novel proposed method for overlapping patches

The testing phase is a fundamental part of the process, as it is where the unlabeled images are verified to check whether they contain cancerous areas or not. For this reason, in this phase, a novel methodology based on confirming the label assigned to each patch using the surrounding overlapping patch labels is proposed (Fig. 5). The mechanism is based on avoiding that the label of a zone being defined only by a single patch containing that zone, but each tissue zone is defined in several patches that overlap here. In this way, several labels of the different patches are present in one area. To corroborate this methodology, a comparison is made between testing these images without overlapping patches or applying an overlap to strengthen the label provided by the network.

In this process for each patch 100 × 100, the surrounding patches are selected that at least share 1/4 of the original patch. In this way, the area to be analyzed contained in the central patch, shares information with 8 patches, see in Fig. 5. If the CNN assigns a label to the zone in question (central patch) this is not considered a good prediction until the process checks the labels of the surrounding patches, and makes a

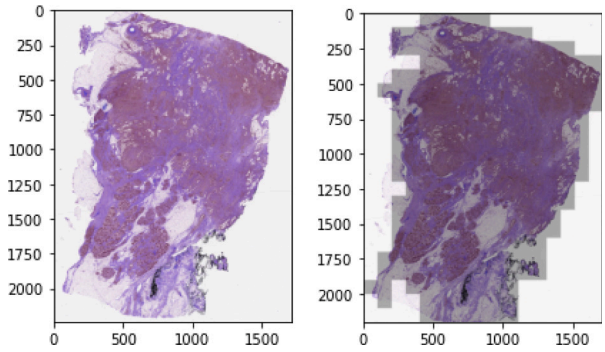

Fig. 4. Tissue region detection by applying the mean of each RGB channel as a threshold. For each patch, the mean of its channels is calculated and decisions are made based on whether the mean of each is greater than 230 or not.

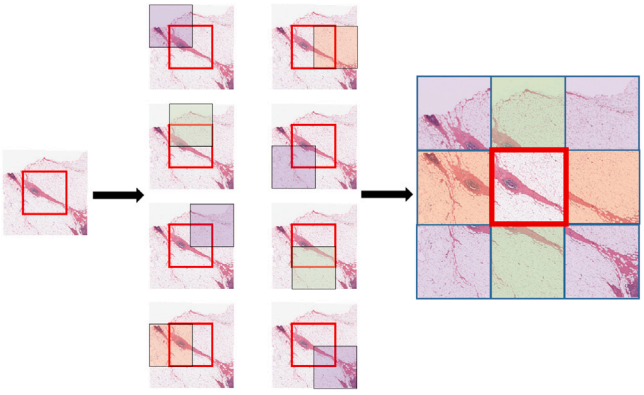

Fig. 5. Overlapping process. For each patch that is in test disposition, not only this patch is evaluated but also the surrounding eight patches that share cells with the parent patch are also evaluated.

decision. In this form, we will try to improve label prediction errors by CNN. In this section, we propose several label assignment alternatives that use this method 4.3.

4.3. Alternatives proffered for label assignment

It is important to explain the process whereby the label is assigned in the test phase. One way to label each zone is by the CNN output of the associated patch [31,33,35,37]. Another alternative is to label each zone not only with the predicted label of the patch itself but also with the labels of neighboring patches that overlap in this zone. For this phase, several alternatives are analyzed in this paper. The alternatives depend on the filters that are applied on the overlapping patches and are as follows:

(a) Filters average-pooling 3 × 3 with stride 2: when this filter is applied, the average labels of the patch in question and the surrounding patches are formed. As the labels are 0 to normal patches and 1 to tumor patches, if the average is equal or higher than 5/9 the patch in question is considered as a patch with tumor tissue, in the contrary case the patch is labeled as normal tissue. For this reason, if 5 of the 9 patches analyzed have a "tumor label", the label on the center patch will be "tumor label". In this alternative, all surrounding patches are considered with the same importance.

(b) Convolutional layer with filter 3 × 3 and stride 2: the convolutions are performed between the predicted labels and the filters. The filters have different weights that you can set depending on the results that you want to get. In this case, the weights of the filters change depending on the positions, i.e., they are set the higher weight to labels of those patches that share more area with the central patch, this can be appreciated in Fig. 6. The filter weights are as follows:

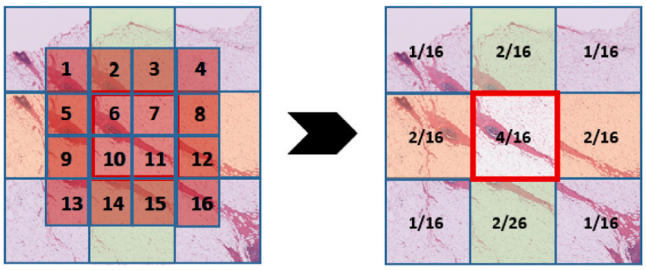

Fig. 6. 3 × 3 filter weights of the convolutional layers.

$$\begin{vmatrix} 1/16 & 2/16 & 1/16 \\ 2/16 & 4/16 & 2/16 \\ 1/16 & 2/16 & 1/16 \end{vmatrix} \quad (1)$$

In this case, the criterion is the same as above but the influence of the filter weight is taken into account. If the mean is greater than 8/16, the patch in question is considered a patch with tumor tissue. Thus, when applying the filter weights, the importance of the central patch is greater than that of the surrounding patches.

(c) Filters average-pooling 2 × 2 with stride 1 plus filters average-pooling 2 × 2 with stride 2: In this case, we evaluate each corner of the central patch separately. First, average-pooling 2 × 2 is applied between the predicted labels of the central patch and the three surrounding patches that are located in each corner. Then, another average-pooling 2 × 2 is applied but with stride 2, being this the filter that calculates the mean of the four corners of a question patch. In this way, the final decision on the label of a patch is made on the basis of the labels of the four corners that were previously evaluated independently. In the first filter, if the mean is greater than 0.5, i.e., more than 2 of the 4 analyzed patches are labeled as a tumor, then the final patch is labeled as a tumor. In the second filter, the threshold is set equal to or higher than 2/4, considering the final patch as a tumor if at least 2 corners have a tumor. Fig. 7 summarizes the complete process where two average-pooling filters are used.

(d) Convolutional layer with filter 2 × 2 and stride 1 plus filters average-pooling 2 × 2 with stride 2: In this case, we evaluate each corner of the central patch individually. First, convolutions are applied between the predicted labels of the central patch and the three surrounding patches at each corner. In this application, the filter weights are as follows in each corner:

$$\begin{array}{cc|cc} 1/9 & 2/9 & 2/9 & 1/9 \\ 2/9 & 4/9 & 4/9 & 2/9 \\ \hline 2/9 & 4/9 & 4/9 & 2/9 \\ 1/9 & 2/9 & 2/9 & 1/9 \end{array}$$

Each corner is assigned different weights because the label of each surrounding patch is considered to have different importance depending on its position in the corner. The threshold for determining whether a corner has a tumor is set to 5/9, i.e. if the convolution output between the filter and the 4 labels is 5/9 or more, it is labeled as a tumour. Next, once each corner is labeled, we apply the average-pooling filter to decide the final patch label. In this last step, the threshold is set to more than 1/4, as we consider the final patch as a tumor if at least 2 corners have a tumor.

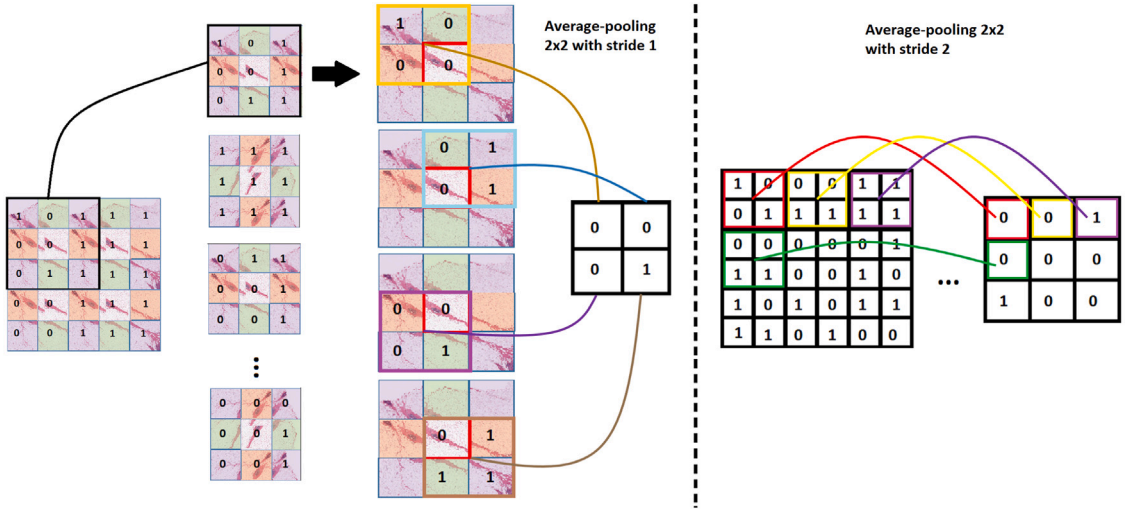

Fig. 7. Process of convolutional layer with filter 2 × 2 and stride 1 plus filters average-pooling 2 × 2 with stride 2.

For this, different alternatives can be studied in this step:

- Non-overlapping method: Normal testing method without the proposed overlap alternative.
- Proposed method:
  - Alternative 1: Testing with overlapping patches, using the filter average-pooling 3 × 3 with stride 2 (alternative (a)).
  - Alternative 2: Testing with overlapping patches, using Convolutional layer with filter 3 × 3 and stride 2 (alternative (b)).
  - Alternative 3: Testing with overlapping patches, using the filter average-pooling 2 × 2 with stride 1 followed by a filter average-pooling 2 × 2 with stride 2 (alternative (c)).
  - Alternative 4: Testing with overlapping patches, using Convolutional layer with filter 2 × 2 and stride 1 plus filters average-pooling 2 × 2 with stride 2 (alternative (d)) (see Table 2).

4.4. Filter to isolation patches

In some cases the prediction of a patch in an area is wrong and this patch is completely surrounded by patches belonging to other classes. On these occasions, it is essential to locate this error and correct the misclassified patch. For this purpose, we use a filter that changes the label of a patch that is surrounded by patches of the other classes, considering that the patch has a classification error. With this technique, we manage to avoid isolated patches in opposite areas where they should be found. This filter indicated above, checks for each patch in question all patches on its sides and changes the label only if all patches are labeled with the opposite label.

4.5. Alteration of CNN threshold

To assign a value to a binary category, a classification threshold (also called a decision threshold) must be established. A value above this threshold means “class 1”, and a value below means “class 2”. It is tempting to assume that the classification threshold must always be 0.5, but the thresholds depend on the problem and are therefore values that must be adjusted. In our application, we start from a threshold of 0.5, but it is interesting to study how raising this value influence in the final performance. Having into account that the normal zone in the images is larger than the tumor zone in most cases, a high threshold is more interesting to make sure that a patch with a tumor is most likely a tumor. In this research, we study 0.5, 0.6 and 0.7 (50%, 60% and 70%) as values of decision threshold.

Table 2
Different alternatives in label assignment.

Method		Filter
Non-overlapping method		–
Proposed	Alternative 1	(a)
	Alternative 2	(b)
	Alternative 3	(c)
	Alternative 4	(d)

5. Results

Note that cross-validation (K-fold) is used in the results, which allows us to make predictions on all our data. The HUP dataset is used for the training, validation, and testing phases. The CINIJ dataset is used for the testing phase only. The HUP dataset is divided into k equal subsets of which k-2 sets are used for training the classifier, and the other 2 are used for the evaluation and testing process (k = 5). Cross-validation is performed for the images and not for the patches since we want to detect for each individual image the location of cancer. For this purpose, it is necessary that the patches of an image that are used in the training phase are not repeated in the validation and training phase, as this would lead to inconsistent results. Therefore, the 5 data splits have the same number of images but not exactly the same number of patches, depending on the size of the images in each split. In the training phase, the CNN is supposed to learn the features of both classes, but in this phase, it is not necessary to use all the patches of each selected image. The methodology used was to avoid class imbalance in the training by choosing the same number of normal class and cancer class patches. In this way, and considering that we had more normal patches, all cancer patches were taken and the same number of normal patches were randomly selected. In the evaluation and testing phases, all the patches of each image belonging to these groups are selected, since it is necessary to evaluate the whole area of the images to locate the areas affected by cancer. The process of selecting the sets is repeated k times, where in each iteration a different set for classifier testing, for evaluation, and the remaining k-2 sets for training. The pre-processing comment in the previous section is applied to the patches obtained.

5.1. Results of patch overlapping

In this phase, the goal is to identify and localize the tumor tissue in Whole images. The parameters examined for the training phase are CNN (Densenet-121, InceptionV3, and VGG16), the optimizers (Adam

Table 3
Classification results for the different methods discussed above (method non-overlapping method and proposed method with overlapping 'alternatives 1-2-3-4'). It shows the misclassified patches (Misl_patc) for both classes, the corrected patches (Corr_patc) with respect to the standard method, and the percentage of correction obtained between the different alternatives and the traditional method.

HUP dataset						
Methods:		Normal tissue		Tumor tissue		Correction %
		Misclassified Patches	Corrected patches	Misclassified Patches	Corrected patches	
Non-overlapping		5040	–	2182	–	
Prop	Alt 1	4159	881	2132	50	12.9
	Alt 2	4251	789	2153	29	11.3
	Alt 3	4058	982	2268	−86	12.4
	Alt 4	4288	752	2271	−89	9.2
CINIJ dataset						
Methods:		Normal tissue		Tumor tissue		Correction %
		Misclassified Patches	Corrected patches	Misclassified Patches	Corrected patches	
Non-overlapping		1199	–	739	–	
Prop	Alt 1	940	259	691	48	15.8
	Alt 2	963	236	710	29	13.7
	Alt 3	917	282	721	18	15.5
	Alt 4	975	224	763	−24	10.3

or SGD), and the number of layers that are trained in the CNN (3 end layers, 30% of layers, and 70% of layers).

At this point, the traditional testing methods are compared with an innovative idea of patch overlapping to improve the prediction labels of each path, using the surrounding patches. As discussed earlier in this report, the combination of parameters that has been best studied is the Densenet-121 architecture with ADAM optimizers and 70% of the total CNN layers trained.

To check the influence of the different alternatives stated above, for the two different datasets, the number of corrected patches is shown compared to the non-overlapping method. The percentage of patches correction of each method is represented in Table 3. The first method refers to the use of the pre-trained CNN to predict the labeling of the different patches in the image, without applying overlaps and filters. The results of this first method are used as a reference to see if the proposed methods improve the traditional prediction result. As can be seen, the table shows the number of corrected patches for each alternative over the proposed method with no overlapping. It can be seen the proposed method, from alternative 1 to alternative 4, improves the number of correct patches. The percentage of correctness, it ranges from 9.2% to 15.8% in the different datasets and proposed alternatives. As can be appreciated in Table 3 the best result is given by alternative 1 of the proposed method.

Fig. 8 shows the summary of cancer prediction in a complete image, from patch selection to determination of the color of the prediction map indicating the area with cancer. As can be seen, the colors range from yellow to red, representing the different cancer probabilities determined by the CNN. Yellow color refers to those patches with a probability greater than 50% and red color refers to those patches with a probability of 100%.

Fig. 11 shows the results of the confusion matrices (CMs) for the different methods introduced in the patch overlapping process. These CMs highlight what has already been mentioned in the tables above, namely that applying the overlap with different filters improves the performance for the classification of the patches in the two classes defined.

Moreover, a comparison between the non-overlapping method and alternative 1 in the proposed method is presented in Fig. 9. This figure shows the prediction map, which indicates well-labeled or poorly labeled patches, and its confusion matrix, where TP, TN, FP, and FN, are located in the image 12 935_idx5 of the HUP dataset. Finally, the confusion matrices of the method without overlapping and alternative 1 (test with overlapping patches, using the 3 × 3 average-pooling filter with stride 2) are shown by this image, showing how the results improve as expected after the results discussed above. Alternative 1 is

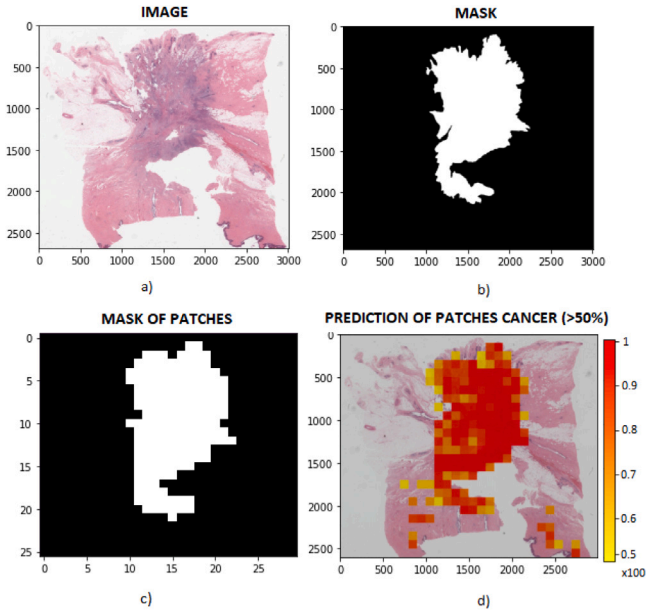

Fig. 8. (a) Image section predicting cancer. (b) Mask associated with the normal and cancer zones. (c) Mask associated with the patches containing tumor cells. (d) Prediction of the zone with tumor by the CNN represented in color according to the percentage of prediction (image 12 894_idx5 of the HUP dataset).

the one shown because, as mentioned above, it provides better results for both classes.

As can be seen in Fig. 9, some mislabeled patches are surrounded by patches of another class. To avoid this, another filter can be applied that changes the label of a patch that is located in an area where all surrounding patches belong to a different class. In this way, we take into account the estimation error for the isolated patches. Therefore, for each patch, the applied filter checks the surrounding patches and changes the label only if all surrounding patches belong to a different class. The effect can be appreciated in Fig. 10 where the isolated patch marked with a black circle is corrected with this alternative. This filter improves the correction of all mislabeled patches around the additional 2%.

Another situation we have observed is the disproportion between the size of the cancerous area and the normal area in the images. Usually, the cancerous area of the tumor is smaller than the normal tissue, which leads to an imbalance in the data and thus the performance

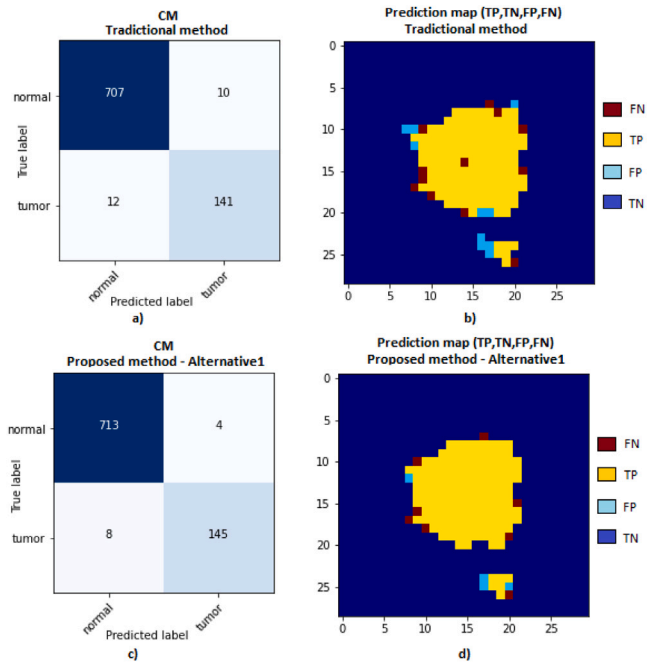

Fig. 9. (a) Confusion matrix for the method without overlapping. (b) Prediction maps of the image in the function of TP(yellow), FN(red), TN(blue), and FP(light blue) for the method without overlapping. (c) Confusion matrix for the proposed method with alternative 1. (d) Prediction maps of the image in the function of TP(yellow), FN(red), TN(blue) and FP(light blue) for the proposed method with alternative 1. (image 12 935_idx5 of the HUP dataset).

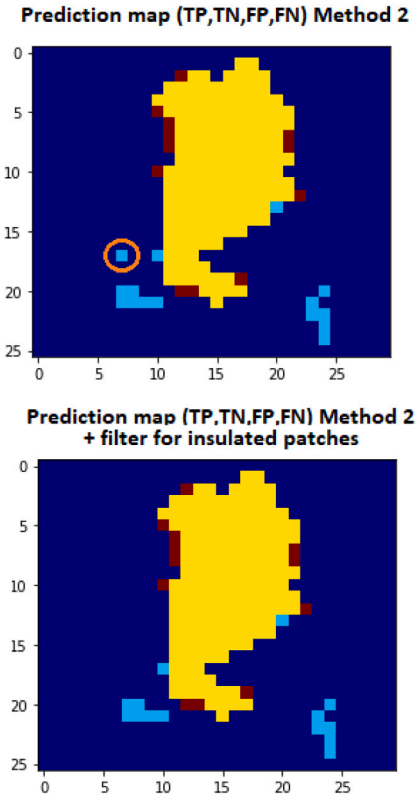

Fig. 10. Correction of isolated patches using a filter that detects when a patch is surrounded by patches of another class.

Table 4
Different alternatives of threshold in method 2.

	Filter	Filter (isolated)	Threshold
Non-overlapping method	–	No	50%
Alternative 1	(a)	No	50%
Alternative 1.1	(a)	Si	50%
Alternative 1.2	(a)	No	60%
Alternative 1.3	(a)	Si	60%
Alternative 1.4	(a)	No	70%
Alternative 1.5	(a)	Si	70%

scores. This imbalance between the two tissue classes in the images may result in a small percentage of mislabeled normal areas but a large impact on the tumor area. To address this, a proposed alternative is to increase the CNN decision threshold to have more confidence in patches labeled as tumors, in exchange for detecting fewer patches. This proposed alternative in conjunction with filters in the overlapping process, allows us to explore new options in the process of detecting cancerous areas in new images. In our application, it is more important to ensure that the patches labeled as tumors are real, in exchange for detecting fewer patches. Therefore, we study the influence of raising the threshold concerning the error in labeling a patch as cancer. This alteration equalizes the number of FN and FP approximately.

In this context, we have investigated increasing the decision threshold from 50% to 60% and 70%, and using the proposed methods and filter to correct for isolated patches. These combinations are compared with previous analyzes using a decision threshold of 50%, their influence on the final performance is investigated. To study the influence of all the above parameters, the proposed method of overlapping with alternative 1 is used, since it gives the best result in the previous analysis. Table 4 summarizes the possible combination that is studied and compared.

The result is presented based on the corrected patches versus the non-overlapping method. These results are represented in the Table 5, which also shows the effect of increasing the threshold on the change in the number of patches in both classes. As explained above, a high threshold results in a lower number of normal patches that are falsely detected as tumors, while the number of tumor patches that are detected as tumors increases. This effect is seen in the table, increasing the erroneous normal patches and decreasing the erroneous tumor patches. For this, can be appreciated some negative values in corrected patches regarding method without overlapping with threshold 50%, being due to changing the number of patches in both classes for a higher threshold.

The final results show that increasing the threshold leads to better results in the evaluation of WSI images. The number of false positives (FPs-misclassified normal patches) decreases, indicating more accuracy in detecting tumor patches, in exchange for sacrificing recall. In other words, we improve performance because, by having more normal patches, we increase the decision threshold for erring on fewer patches of this class in exchange for slightly worse detection of tumor patches. The final results show that using this metric together with the proposed alternative 1 and the filter for isolated patches we were able to correct 20% of the patches that were mislabeled in the alternative without overlapping, increasing the final accuracy of the environment to 2%.

6. Conclusion

In this paper, a new approach for cancer zone detection in whole images is presented. For this purpose, the whole slide image (WSI) and the tumor mask associated with each of these images are used.

The study begins by creating a patch dataset with two classes ‘tumor’ and ‘normal’ by using the mask to differentiate the different zones in the images. The patch dataset is then used in the training phase, to obtain the decision of CNN about the different label patches.

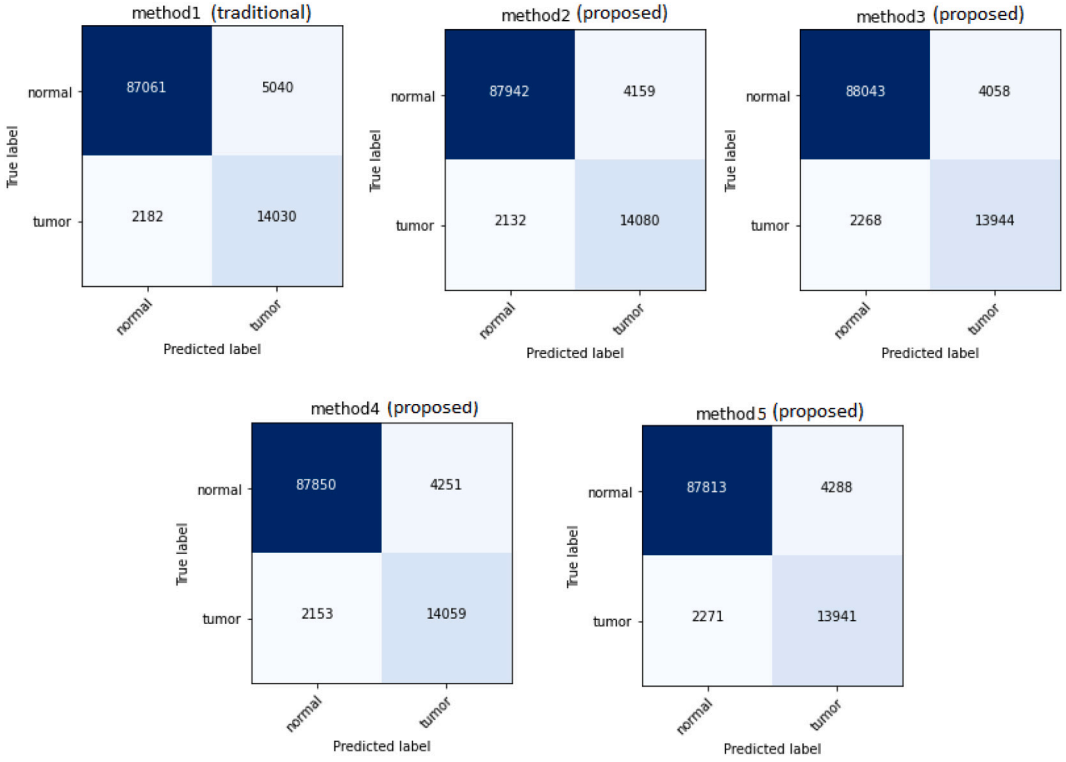

Fig. 11. Confusion matrixes about the different methods treaties during this research for HUP dataset.

Table 5
Classification results using different thresholds in the alternative 1 of the method proposed. It shows the mislabeled patches for both classes (Misl_patc), the corrected patches (Corr_patc), the total corrected patches (T_Corr_patc), and the percentage of correction obtained (Correction %) between the variation of alternative 1 of the method proposed and the traditional method).

HUP dataset								
Methods:		Normal patches (92 101)		Tumor patches (16 212)		TOTAL		
		Misl_patc	Corr_patc	Misl_patc	Corr_patc	T_Corr_patc	Correction %	Accuracy
Non-overlapping method		5040	–	2182	–	–	–	93.3
Proposed overlapping method	Alt 1	4159	881	2132	50	931	12.9	94.2
	Alt 1.1	4063	977	2139	43	1200	16.6	94.3
	Alt 1.2	3404	1636	2598	−416	1220	16.9	94.4
	Alt 1.3	3327	1713	2611	−429	1284	17.8	94.5
	Alt 1.4	2443	2597	3432	−1250	1347	18.6	94.6
	Alt 1.5	2385	2655	3444	−1262	1393	19.3	94.6
CINIJ dataset								
Methods:		Normal patches (13 894)		Tumor patches (4684)		TOTAL		
		Misl_patc	Corr_patc	Misl_patc	Corr_patc	T_Corr_patc	Correction %	Accuracy
Non-overlapping method		1199	–	739	–	–	–	89.6
Proposed overlapping method	Alt 1	940	259	691	48	307	15.8	91.2
	Alt 1.1	918	281	688	51	332	17.1	91.4
	Alt 1.2	718	481	818	−79	402	20.7	91.7
	Alt 1.3	700	499	817	−78	421	21.7	91.8
	Alt 1.4	468	731	1095	−356	375	19.3	91.5
	Alt 1.5	466	733	1090	−351	382	19.7	91.6

Then, to improve the prediction of cancer zones, a novel patch overlap approach is proposed. In this method, several alternatives are proposed using different filters to determine the final label of a studied area. Four alternatives are compared again to the method without overlapping to label a zone, improving the result in each case. A filter is also applied to correct the isolated mislabeled patches, achieving a correction of about 2% of the total mislabeled patches. In addition, it is found that varying the CNN decision threshold can be beneficial in reducing false labels in tumor prediction. In this way, due to class imbalance in the images, the precision and recall markers are equalized. These CNN decision thresholds are investigated in alternative 1 which provides the best results. Comparing the correction results of the patches concerning the non-overlapping method, we reach about 20% correction concerning the method without overlapping.

It can be concluded that the new method proposed in this study, based on overlapping of the patches, with the appropriate filters and adjusting the decision threshold to determine the cancer area, significantly improves the prediction results of the conventional non-overlapping method.

CRediT authorship contribution statement

Sergio Ortiz: Conceptualization, Methodology, Software, Validation, Formal analysis, Investigation, Resources, Writing – original draft, Writing – review & editing. **Ignacio Rojas-Valenzuela:** Methodology, Validation, Formal analysis, Investigation, Writing – review & editing. **Fernando Rojas:** Methodology, Validation, Formal analysis, Investigation, Supervision. **Olga Valenzuela:** Methodology, Validation, Formal analysis, Investigation, Supervision. **Luis Javier Herrera:** Methodology, Validation, Formal analysis, Investigation, Supervision. **Ignacio Rojas:** Conceptualization, Methodology, Validation, Formal analysis, Investigation, Writing – original draft, Writing – review & editing, Supervision, Project administration, Funding acquisition.

Declaration of competing interest

The authors declare that they have no known competing financial interests or personal relationships that could have appeared to influence the work reported in this paper.

Funding

This work has been partially supported by the Project PID2021-128317OB-I0, funded by the MCIN/AEI/ 10.13039/501100011033 and "ERDF A way of making Europe". Funding for open access charge: Universidad de Granada / CBUA. All authors approved the final version of manuscript to be published.

References

[1] C. Fitzmaurice, et al., Global, regional, and national cancer incidence, mortality, years of life lost, years lived with disability, and disability-adjusted life-years for 29 cancer groups, 1990 to 2017: a systematic analysis for the global burden of disease study, JAMA Oncol. (2019).

[2] World-Health-Organization, Estimated number of new cases from 2020 to 2040, incidence, both sexes, age [0-85+], Int. Agency Res. Cancer (2022).

[3] R.A. Neumüller, J.A. Knoblich, Dividing cellular asymmetry: asymmetric cell division and its implications for stem cells and cancer, Genes Dev. 23 (23) (2009) 2675–2699.

[4] R.L. Siegel, K.D. Miller, H.E. Fuchs, A. Jemal, Cancer statistics, 2022, CA: Cancer J. Clin. 72 (1) (2022) 7–33, http://dx.doi.org/10.3322/caac.21708.

[5] H. Sung, J. Ferlay, R.L. Siegel, M. Laversanne, I. Soerjomataram, A. Jemal, F. Bray, Global cancer statistics 2020: GLOBOCAN estimates of incidence and mortality worldwide for 36 cancers in 185 countries, CA: Cancer J. Clin. 71 (3) (2021) 209–249.

[6] R.L. Siegel, K.D. Miller, N.S. Wagle, A. Jemal, Cancer statistics, 2023, CA: Cancer J. Clin. 73 (1) (2023) 17–48, http://dx.doi.org/10.3322/caac.21763.

[7] F. Bray, J. Ferlay, I. Soerjomataram, R.L. Siegel, L.A. Torre, A. Jemal, Global cancer statistics 2018: GLOBOCAN estimates of incidence and mortality worldwide for 36 cancers in 185 countries, CA: Cancer J. Clin. 68 (6) (2018) 394–424.

[8] M. Veta, J.P. Pluim, P.J. Van Diest, M.A. Viergever, Breast cancer histopathology image analysis: A review, IEEE Trans. Biomed. Eng. 61 (5) (2014) 1400–1411.

[9] M. Obayya, M.S. Maashi, N. Nemri, H. Mohsen, A. Motwakel, A.E. Osman, A.A. Alneil, M.I. Alsaid, Hyperparameter optimizer with deep learning-based decision-support systems for histopathological breast cancer diagnosis, Cancers 15 (3) (2023) 885, http://dx.doi.org/10.3390/cancers15030885.

[10] Y.-J. Li, H.-H. Chou, P.-C. Lin, M.-R. Shen, S.-Y. Hsieh, A novel deep learning-based algorithm combining histopathological features with tissue areas to predict colorectal cancer survival from whole-slide images, J. Transl. Med. 21 (1) (2023) http://dx.doi.org/10.1186/s12967-023-04530-8.

[11] S. Kothari, J.H. Phan, T.H. Stokes, M.D. Wang, Pathology imaging informatics for quantitative analysis of whole-slide images, J. Amer. Med. Inform. Assoc. 20 (6) (2013) 1099–1108.

[12] C. Daniel, M.G. Rojo, J. Klossa, V. Della Mea, D. Booker, B.A. Beckwith, T. Schrader, Standardizing the use of whole slide images in digital pathology, Comput. Med. Imaging Graph. 35 (7–8) (2011) 496–505.

[13] D. Crosby, S. Bhatia, K.M. Brindle, L.M. Coussens, C. Dive, M. Emberton, S. Esener, R.C. Fitzgerald, S.S. Gambhir, P. Kuhn, T.R. Rebbeck, S. Balasubramanian, Early detection of cancer, Science 375 (6586) (2022).

[14] R.C. Fitzgerald, A.C. Antoniou, L. Fruk, N. Rosenfeld, The future of early cancer detection, Nat. Med. 28 (4) (2022) 666–677.

[15] S. Martino, C. Tammaro, G. Misso, M. Falco, M. Scrima, M. Bocchetti, I. Rea, L.D. Stefano, M. Caraglia, microRNA detection via nanostructured biochips for early cancer diagnostics, Int. J. Mol. Sci. 24 (9) (2023) 7762, http://dx.doi.org/10.3390/ijms24097762.

[16] Y.E. Almalki, T.A. Soomro, M. Irfan, S.K. Alduraibi, A. Ali, Computerized analysis of mammogram images for early detection of breast cancer, Healthcare 10 (5) (2022) 801.

[17] T. Liu, R. Su, C. Sun, X. Li, L. Wei, EOCSA: Predicting prognosis of epithelial ovarian cancer with whole slide histopathological images, Expert Syst. Appl. 206 (2022) 117643.

[18] C. Zhang, Y. Bai, C. Yang, R. Cheng, X. Tan, W. Zhang, G. Zhang, Histopathological image recognition of breast cancer based on three-channel reconstructed color slice feature fusion, Biochem. Biophys. Res. Commun. 619 (2022) 159–165, http://dx.doi.org/10.1016/j.bbrc.2022.06.004.

[19] K. Huang, B. Lin, J. Liu, Y. Liu, J. Li, G. Tian, J. Yang, Predicting colorectal cancer tumor mutational burden from histopathological images and clinical information using multi-modal deep learning, Bioinformatics (2022).

[20] P. Alirezazadeh, F. Dornaika, Boosted additive angular margin loss for breast cancer diagnosis from histopathological images, Comput. Biol. Med. 166 (2023) 107528, http://dx.doi.org/10.1016/j.compbiomed.2023.107528.

[21] N. Pashayan, P.D.P. Pharoah, The challenge of early detection in cancer, Science 368 (6491) (2020) 589–590, http://dx.doi.org/10.1126/science.aaz2078.

[22] C. Zhang, N. Bao, H. Sun, H. Li, J. Li, W. Qian, S. Zhou, A deep learning image data augmentation method for single tumor segmentation, Front. Oncol. 12 (2022) http://dx.doi.org/10.3389/fonc.2022.782988.

[23] E. Adams, G.D. Sepich-Poore, S. Miller-Montgomery, R. Knight, Using all our genomes: Blood-based liquid biopsies for the early detection of cancer, View 3 (1) (2022) 20200118, http://dx.doi.org/10.1002/viw.20200118.

[24] E. Chartampilas, V. Rafailidis, V. Georgopoulou, G. Kalarakis, A. Hatzidakis, P. Prassopoulos, Current imaging diagnosis of hepatocellular carcinoma, Cancers 14 (16) (2022) 3997, http://dx.doi.org/10.3390/cancers14163997.

[25] N. Khanam, R. Kumar, Recent applications of artificial intelligence in early cancer detection, Curr. Med. Chem. 29 (25) (2022) 4410–4435.

[26] X. Meng, T. Zou, Clinical applications of graph neural networks in computational histopathology: A review, Comput. Biol. Med. 164 (2023) 107201, http://dx.doi.org/10.1016/j.compbiomed.2023.107201.

[27] V.S. Srikanth, S. Krithiga, Pre-trained deep neural network-based computer-aided breast tumor diagnosis using ROI structures, Intell. Autom. Soft Comput. 35 (1) (2023) 63–78, http://dx.doi.org/10.32604/iasc.2023.023474.

[28] Ü. Budak, Z. Cömert, Z.N. Rashid, A. Şengür, M. Çıbuk, Computer-aided diagnosis system combining FCN and bi-LSTM model for efficient breast cancer detection from histopathological images, Appl. Soft Comput. 85 (2019) 105765, http://dx.doi.org/10.1016/j.asoc.2019.105765.

[29] R.M. Rangayyan, F.J. Ayres, J.L. Desautels, A review of computer-aided diagnosis of breast cancer: Toward the detection of subtle signs, J. Franklin Inst. B 344 (3–4) (2007) 312–348, http://dx.doi.org/10.1016/j.jfranklin.2006.09.003.

[30] L. Duran-Lopez, J.P. Dominguez-Morales, A.F. Conde-Martin, S. Vicente-Diaz, A. Linares-Barranco, PROMETEO: A CNN-based computer-aided diagnosis system for WSI prostate cancer detection, IEEE Access 8 (2020) 128613–128628, http://dx.doi.org/10.1109/access.2020.3008868.

[31] A. Cruz-Roa, H. Gilmore, A. Basavanhally, M. Feldman, S. Ganesan, N.N. Shih, J. Tomaszewski, F.A. González, A. Madabhushi, Accurate and reproducible invasive breast cancer detection in whole-slide images: A deep learning approach for quantifying tumor extent, Sci. Rep. 7 (1) (2017) 1–14.

[32] D. Wang, A. Khosla, R. Gargeya, H. Irshad, A.H. Beck, Deep learning for identifying metastatic breast cancer, 2016, arXiv preprint arXiv:1606.05718.

[33] S. Dabeer, M.M. Khan, S. Islam, Cancer diagnosis in histopathological image: CNN based approach, Inform. Med. Unlocked 16 (2019) 100231.

[34] K. Fan, S. Wen, Z. Deng, Deep learning for detecting breast cancer metastases on WSI, in: Innovation in Medicine and Healthcare Systems, and Multimedia, Springer, 2019, pp. 137–145.

[35] E. Deniz, A. Şengür, Z. Kadiroğlu, Y. Guo, V. Bajaj, Ü. Budak, Transfer learning based histopathologic image classification for breast cancer detection, Health Inf. Sci. Syst. 6 (1) (2018) 1–7.

[36] S. Sharma, R. Mehra, Conventional machine learning and deep learning approach for multi-classification of breast cancer histopathology images—a comparative insight, J. Digit. Imaging 33 (3) (2020) 632–654.

[37] K. Das, S. Conjeti, J. Chatterjee, D. Sheet, Detection of breast cancer from whole slide histopathological images using deep multiple instance CNN, IEEE Access 8 (2020) 213502–213511.

[38] M. Toğaçar, K.B. Özkurt, B. Ergen, Z. Cömert, BreastNet: A novel convolutional neural network model through histopathological images for the diagnosis of breast cancer, Physica A 545 (2020) 123592, http://dx.doi.org/10.1016/j.physa.2019.123592.

[39] M. Gour, S. Jain, T.S. Kumar, Residual learning based CNN for breast cancer histopathological image classification, Int. J. Imaging Syst. Technol. 30 (3) (2020) 621–635, http://dx.doi.org/10.1002/ima.22403, URL https://doi.org/10.1002/ima.22403.

[40] L. Li, X. Pan, H. Yang, Z. Liu, Y. He, Z. Li, Y. Fan, Z. Cao, L. Zhang, Multi-task deep learning for fine-grained classification and grading in breast cancer histopathological images, Multimedia Tools Appl. 79 (21–22) (2018) 14509–14528, http://dx.doi.org/10.1007/s11042-018-6970-9.

[41] V.K. Reshma, N. Arya, S.S. Ahmad, I. Wattar, S. Mekala, S. Joshi, D. Krah, Detection of breast cancer using histopathological image classification dataset with deep learning techniques, BioMed Res. Int. 2022 (2022) 1–13, http://dx.doi.org/10.1155/2022/8363850.

[42] Z. Hu, J. Tang, Z. Wang, K. Zhang, L. Zhang, Q. Sun, Deep learning for image-based cancer detection and diagnosis–A survey, Pattern Recognit. 83 (2018) 134–149, http://dx.doi.org/10.1016/j.patcog.2018.05.014.

[43] L. Cong, W. Feng, Z. Yao, X. Zhou, W. Xiao, Deep learning model as a new trend in computer-aided diagnosis of tumor pathology for lung cancer, J. Cancer 11 (12) (2020) 3615–3622, http://dx.doi.org/10.7150/jca.43268.

[44] N. Coudray, P.S. Ocampo, T. Sakellaropoulos, N. Narula, M. Snuderl, D. Fenyö, A.L. Moreira, N. Razavian, A. Tsirigos, Classification and mutation prediction from non–small cell lung cancer histopathology images using deep learning, Nat. Med. 24 (10) (2018) 1559–1567, http://dx.doi.org/10.1038/s41591-018-0177-5.

[45] F.A. Spanhol, L.S. Oliveira, C. Petitjean, L. Heutte, Breast cancer histopathological image classification using convolutional neural networks, in: 2016 International Joint Conference on Neural Networks (IJCNN), IEEE, 2016, http://dx.doi.org/10.1109/ijcnn.2016.7727519.

[46] K. Dimitropoulos, P. Barmpoutis, C. Zioga, A. Kamas, K. Patsiaoura, N. Grammalidis, Grading of invasive breast carcinoma through grassmannian VLAD encoding, PLoS One 12 (9) (2017) e0185110, http://dx.doi.org/10.1371/journal.pone.0185110.

[47] A. Janowczyk, A. Madabhushi, Deep learning for digital pathology image analysis: A comprehensive tutorial with selected use cases, J. Pathol. Inform. 7 (1) (2016) 29, http://dx.doi.org/10.4103/2153-3539.186902.

[48] M. Alruwaili, W. Gouda, Automated breast cancer detection models based on transfer learning, Sensors 22 (3) (2022) 876, http://dx.doi.org/10.3390/s22030876.

[49] Y.J. Kim, E.Y. Yoo, K.G. Kim, Deep learning based pectoral muscle segmentation on mammographic image analysis society (MIAS) mammograms, Precis. Future Med. (2021) http://dx.doi.org/10.23838/pfm.2020.00170.

[50] A. Cruz-Roa, H. Gilmore, A. Basavanhally, M. Feldman, S. Ganesan, N. Shih, J. Tomaszewski, A. Madabhushi, F. González, Data from: High-throughput adaptive sampling for whole-slide histopathology image analysis (HASHI) via convolutional neural networks: application to invasive breast cancer detection, 2018, http://dx.doi.org/10.5061/DRYAD.1G2NT41, URL https://datadryad.org/stash/dataset/doi:10.5061/dryad.1g2nt41.

[51] M. Babawale, A. Gunavardhan, J. Walker, T. Corfield, P. Huey, A. Savage, A. Bansal, M. Atkinson, H. Abdelsalam, E. Raweily, A. Christian, I. Evangelou, D. Thomas, J. Shannon, E. Youd, P. Brumwell, J. Harrison, I. Thompson, M. Rashid, G. Leopold, A. Finall, S. Roberts, D. Housa, P. Nedeva, A. Davies, D. Fletcher, M. Aslam, Verification and validation of digital pathology (whole slide imaging) for primary histopathological diagnosis: All Wales experience, J. Pathol. Inform. 12 (1) (2021) 4, http://dx.doi.org/10.4103/jpi.jpi_55_20.

[52] G. Huang, Z. Liu, L. Van Der Maaten, K.Q. Weinberger, Densely connected convolutional networks, in: Proceedings of the IEEE Conference on Computer Vision and Pattern Recognition, 2017, pp. 4700–4708.

[53] Y. Zhu, S. Newsam, Densenet for dense flow, in: 2017 IEEE International Conference on Image Processing (ICIP), IEEE, 2017, pp. 790–794.

[54] U. Ruby, V. Yendapalli, Binary cross entropy with deep learning technique for image classification, Int. J. Adv. Trends Comput. Sci. Eng. 9 (10) (2020).